Hydroxyl Radical Adducts to Pyridine. The Generation and Properties of the Elusive *N*-Hydroxypyridyl Radical

Shetty Vivekananda, Jill K. Wolken, and František Tureček*

Department of Chemistry, Bagley Hall, Box 351700, University of Washington, Seattle, Washington 98195-1700

Received: March 5, 2001; In Final Form: July 24, 2001

The elusive *N*-hydroxypyridyl radical **1** has been generated transiently in the gas phase by collisional neutralization of the stable cation $\mathbf{1}^+$. The radical underwent extensive dissociation by specific losses of H, OH, and ring-cleavage reactions, as elucidated by neutralization-reionization mass spectrometry aided by deuterium labeling. Effective QCISD(T)/6-311+G(3df,2p) and combined Møller−Plesset and density functional theory calculations indicated that loss of OH from **1** was 49 kJ mol^{-1} exothermic and proceeded on the potential energy surface of the ground doublet electronic state of the radical. The loss of H and ring-cleavage dissociations were initiated by the formation of excited electronic states in **1** that provided the internal energy for these endothermic reactions. OH radical addition to pyridine was predicted by transition-state theory calculations to occur mainly (82%) in the C-3 and C-5 positions. Hydrogen atom addition to pyridine-*N*-oxide (**2**) was predicted to occur selectively at the oxygen atom and trigger a reaction sequence that can result in a highly exothermic catalytic isomerization of **2** to hydroxypyridines.

Introduction

Additions of small radicals to aromatic and heteroaromatic systems represent the kinetically important steps in chemical processes as diverse as tropospheric oxidation,[1] pulse radiolysis,[2] and radiation and oxidative damage.[3] While the kinetics of radical additions can be studied and stable addition products can be analyzed under carefully controlled conditions, the identity and chemical properties of transient radical intermediates are difficult to elucidate directly in situ. In particular, additions to pyridine by hydroxyl radicals produced by pulse radiolysis have been studied and isomeric hydroxypyridines have been isolated as stable products.[4] However, much less is known about the mechanism and energetics of the additions, including the structures and relative stabilities of transient adducts, and activation energies for the additions. Pyridine is substantially less reactive than benzene toward electrophilic additions.[5] The reactivity toward electrophilic attack at the different sites in pyridine decreases in the series N-1 ≫ C-3/C-5 > C-4 > C-2/C-6 due to the electron-withdrawing effect of the nitrogen atom.[5] Since the hydroxyl radical is an open-shell electrophile, the relative rates of addition to the different positions in pyridine are of relevance with respect to the general question of pyridine reactivity in both electrophilic and radical additions. Early ab initio calculations[6] indicated that OH should attack pyridine in the C-3/C-5 positions, in keeping with pulse radiolysis experiments in aqueous solution.[4c] However, OH reactions with pyridine showed vastly different rate constants in the gas-phase[1,7] and solution,[4b] which raised the possibility of different reaction mechanisms and reactive intermediates being involved in the gas-phase reaction.

We have shown previously[8] that transient radical adducts to aromatic and heterocyclic systems can be generated and studied in the gas phase using neutralization-reionization mass spectrometry.[9] This comprises the generation of a stable gas-phase ion, which is selected and accelerated to a high velocity, e.g., 129 000 m s^{-1} for the charged pyridine-hydroxyl adducts described below. The fast ion is discharged by a glancing collision with a polarizable molecular donor (trimethylamine, dimethyl disulfide, etc.) and the newly formed radicals are separated electrostatically from remaining precursor ions. Transfer of an electron from the thermal electron donor to the fast ion occurs over a distance of a few molecular diameters (5−10 Å), which limits the time scale for the electron transfer to <8 fs. This implies that the nascent radical is formed with the structure and nearly identical geometry of the precursor ion, because the time for the electron transfer is shorter than the periods of molecular vibrations. Unimolecular dissociations of transient radicals are then studied on a microsecond time scale (e.g., 4.7 μs for the pyridine−hydroxyl adducts), and the undissociated radicals and dissociation products are collisionally ionized and analyzed by mass spectrometry.

Here we report on the transient generation of the hitherto elusive adduct of hydroxyl radical to N-1 in pyridine (**1**). We studied the formation and unimolecular dissociations of **1** and also carried out extensive ab initio and combined density functional theory and perturbational calculations of energies for the pyridine-hydroxyl adduct **1**, several cyclic isomers (**3**−**9**), ring-cleavage intermediates (**10**−**12**), transition states, and dissociation products. We show, inter alia, that the formation of **1** by collisional electron-transfer involves excited electronic states that affect the radical dissociations.

Experimental Section

Methods. Measurements were carried out on a tandem quadrupole acceleration−deceleration mass spectrometer described previously.[10] The pyridine-*N*-oxide cation radical ($\mathbf{2}^{+\bullet}$) was generated in a standard electron ionization source. Typical ionization conditions were as follows: electron energy 70 eV,

* Corresponding author. Department of Chemistry, Bagley Hall, Box 351700, University of Washington, Seattle, WA 98195-1700. Tel.: (206) 685-2041. Fax: (206) 685-3478. E-mail: turecek@chem.washington.edu..

10.1021/jp010844k CCC: $20.00
Published on Web 09/08/2001

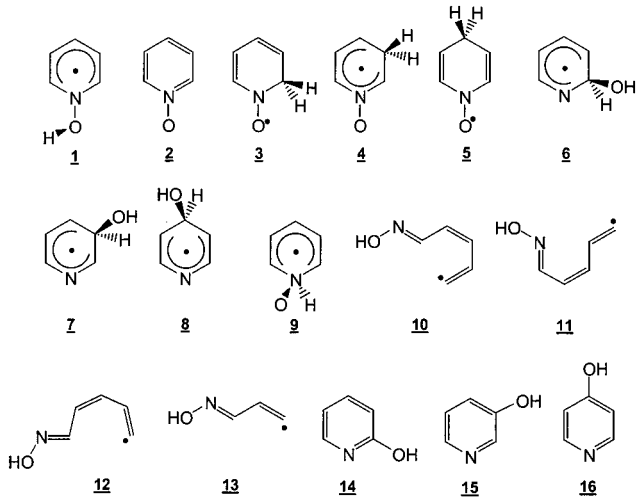

emission current 500 μA, temperature 200−250 °C. Ion−molecule reactions were used to generate ions $\mathbf{1}^+$ and $\mathbf{1a}^+$ in a tight chemical ionization (CI) source. Typical ionization conditions were as follows: electron energy 100 eV, emission current 1−2 mA, temperature 280−300 °C, ion source potential 80 V. NH_3, ND_3, acetone, and CD_3COCD_3 were used as CI reagent gases at pressures of $1.0-1.5 \times 10^{-4}$ Torr, as read on an ionization gauge located at the diffusion pump intake. Stable precursor ions were passed through a quadrupole mass filter operated in the radio frequency-only mode, accelerated to the total kinetic energy of 8250 eV and neutralized in the collision cell floated at −8170 V. The precursor ion lifetimes were 30−40 μs. Dimethyl disulfide (DMDS) was admitted to the differentially pumped collision cell at a pressure such as to achieve 70% transmittance of the precursor ion beam. The ions and neutrals were allowed to drift to a four segment conduit,[11] where the ions were reflected by the first segment floated at +250 V. The neutral flight times in standard NRMS measurements were 4.6 μs. The fast neutral species were reionized in the second collision cell with oxygen or nitrogen dioxide at pressures adjusted such as to achieve 70% transmittance of the precursor ion beam. The ions formed in the second collision cell were decelerated, energy filtered, and analyzed by a quadrupole mass filter operated at unit mass resolution. The instrument was tuned daily to maximize the ion current of reionized $CS_2^{+\bullet}$. Typically, 40 repetitive scans were accumulated per spectrum, and each spectrum was reproduced at least three times over a period of several weeks.

Collisionally activated dissociation (CAD) spectra were measured on a JEOL HX-110 double-focusing mass spectrometer of forward geometry (the electrostatic sector E precedes the magnet B). Collisions with air were monitored in the first field-free region at pressures such as to achieve 70% transmittance of the ion beam at 10 keV. The spectra were obtained by scanning E and B simultaneously while maintaining a constant *B*/*E* ratio (*B*/*E* linked scan).

Calculations. Standard ab initio and density functional theory calculations were performed using the Gaussian 98 suite of programs.[12] Geometries were optimized using Becke's hybrid functional (B3LYP)[13] and the 6-31+G(d,p) basis set. Spin-unrestricted calculations (UB3LYP and UMP2) were used for open-shell systems. Spin contamination in the UB3LYP calculations was small as judged from the $\langle S^2 \rangle$ operator expectation values that were 0.75−0.77. The optimized structures were characterized by harmonic frequency analysis as local minima (all frequencies real) or first-order saddle points (one imaginary frequency). Complete optimized structures in the Cartesian coordinate format and harmonic frequencies are available from the correspondence author upon request. The B3LYP/6-31+G-(d,p) frequencies were scaled by 0.963 (ref 14, for other scaling factors see ref 15) and used to calculate zero-point vibrational energies (ZPVE), enthalpy corrections, and partition functions. The rigid-rotor harmonic oscillator approximation was used in all thermochemical calculations. Single-point energies were calculated at several levels of theory. In two sets of calculations, MP2(frozen core)[16] and B3LYP energies were calculated with basis sets of increasing size, e.g., 6-311+G(2d,p) and 6-311+G-(3df,2p). A complete set of total energies can be obtained from the correspondence author upon request. Spin contamination in the UMP2 calculations was substantial for radicals and transition states, as evidenced by the spin expectation values $\langle S^2 \rangle$ that ranged between 0.77 and 1.673, but showed only a weak dependence on the basis set used. Spin annihilation using Schlegel's projection method[17] (PMP2)[12] reduced the $\langle S^2 \rangle$ values to 0.75−1.526 and resulted in total energy decrease by 23−51 millihartree In addition, restricted open-shell (ROMP2) calculations[18] were carried out for the entire set of structures to deal with spin contamination.[19] The PMP2 and ROMP2 energies were averaged with the B3LYP energies according to the empirical procedure that was introduced previously[20] and tested for several systems since.[21,22] This resulted in error cancellation and provided relative energies denoted as B3-PMP2 or B3-ROMP2,[21,22] as discussed below. Calculations on closed-shell systems are marked by B3-MP2. In addition, a composite procedure was adopted that consisted of a single-point quadratic configuration interaction calculation,[23] QCISD(T)/6-31G(d,p), and basis set expansion up to 6-311+G(3df,2p) through PMP2 or ROMP2 single-point calculations according to eq 1:

$$\text{QCISD(T)/6-311+G(3df,2p)} \approx \text{QCISD(T)/6-31G(d,p)} + \text{MP2/6-311 + G(3df,2p)} - \text{MP2/6-31G(d,p)} \quad (1)$$

This level of theory is intermediate between those of the Gaussian 2 (MP2) method[24] which uses the 6-311G(d,p) basis set in the large QCISD(T) calculation and the G2(MP2, SVP) method[25] which uses the 6-31G(d) basis set instead. Spin contamination in the effective QCISD(T) energies was small (1.8 millihartree root-mean-square deviation upon spin annihilation) because of an efficient cancellation of spin effects on the MP2 terms. We also utilized the previous finding that restricted open-shell calculations (ROMP2) provided good stabilization energies for small organic radicals.[19] The calculated total energies are available from the authors upon request.

Franck−Condon energies in vertical neutralization and reionization were taken as absolute differences between the total B3-MP2/6-311+G(2d,p) energies of fully optimized ion or neutral structures and those in which an electron has been added to an optimized cation structure or subtracted from an optimized neutral structure. No zero-point corrections were applied to the calculated Franck−Condon energies.

Gradient optimizations of excited-state geometries were performed with spin-unrestricted configuration interaction singles (UCIS)[26] using the 6-31+G(d,p) basis set. Improved energies for excited states were obtained from UCIS and time-dependent density functional theory[27] single-point calculations using the B3LYP hybrid functional and the larger 6-311+G(2d,p) basis set. These calculations are denoted by TD-B3LYP.

Results and Discussion

Formation of 1. Radical **1** was generated by the reaction sequence shown in Scheme 1. First, cation $\mathbf{1}^+$ was produced

SCHEME 1

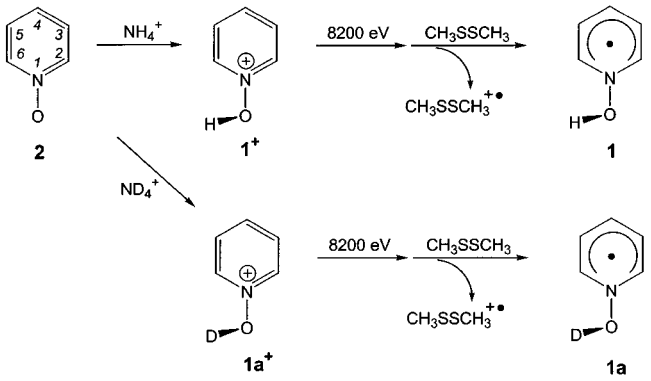

TABLE 1: Proton Affinities and Ionization Energies

species/reaction	energy[a] B3-MP2 6-311+G(3df,2p)	energy[a] QCISD(T)[b] 6-311+G(3df,2p)
$\mathbf{1}^+ \rightarrow \mathbf{2} + H^+$	914	920
$\mathbf{3}^+ \rightarrow \mathbf{2} + H^+$	753	
$\mathbf{4}^+ \rightarrow \mathbf{2} + H^+$	656	
$\mathbf{5}^+ \rightarrow \mathbf{2} + H^+$	761	
$\mathbf{1} \rightarrow \mathbf{1}^+$	516[c]	509[c]
	523	517
$\mathbf{2} \rightarrow \mathbf{2}^{+\bullet}$	816[c]	810[c]
	821	807

[a] In units of kJ mol^{-1} at 298 K. [b] Effective energies from basis set expansions. [c] PMP2 data in upper lines, ROMP2 data in lower lines.

selectively by gas-phase protonation of pyridine-*N*-oxide (**2**). Since the oxygen atom is the most basic site in **2**,[28] it is selectively protonated with gas-phase acids (BH^+) of proton affinities, PA(B), in the range of 760−920 kJ mol^{-1}, such as NH_4^+ ($PA(NH_3)$ = 853 kJ mol^{-1}) and $(CH_3)_2COH^+$ (PA(acetone) = 821 kJ mol^{-1}).[29] Likewise, ND_4^+ and $(CD_3)_2COD^+$ were used for selective deuteronation at oxygen to generate ion $\mathbf{1a}^+$ (Scheme 1). The topical proton affinities of the less basic sites in **2**, e.g., C-2 (forming $\mathbf{3}^+$), C-3 (forming $\mathbf{4}^+$), and C-4 (forming $\mathbf{5}^+$), are summarized in Table 1.

Neutralization of $\mathbf{1}^+$ followed by reionization resulted in substantial dissociation, as shown in Figure 1a. The NR spectrum of $\mathbf{1}^+$ showed a peak at *m*/*z* 96 that coincided by mass with the survivor ion $\mathbf{1}^+$. However, the apparent survivor ion in the NR spectrum of $\mathbf{1}^+$ was, to a large extent, due to an isobaric interference of ca. 2.3% of combined ^{13}C and ^{15}N isotopomers of $\mathbf{2}^{+\bullet}$ at *m*/*z* 96 which was not resolved from $\mathbf{1}^+$ in the precursor ion beam (see inset in Figure 1a). Note that the reference NR spectrum of $\mathbf{2}^{+\bullet}$ showed a very prominent survivor ion (Figure 2a). In the absence of isotopic interference the survivor ion of $\mathbf{1}^+$ was very weak. The NR spectrum of the deuteronated ion $\mathbf{1a}^+$ (Figure 1b) showed *a very weak survivor ion*, in keeping with the negligible interference from combined ^{13}C, ^{15}N, and ^{18}O isotope contributions (0.05% combined) at *m*/*z* 97 in the precursor ion beam (Figure 1b, inset). With regard to the substantial thermodynamic stability of $\mathbf{1}^+$ (vide infra), the absence of a survivor ion can be unambiguously ascribed to the low stability of radical **1**.

Dissociations of 1. The main dissociations of **1** upon NR were ring cleavages that produced overlapping $C_4H_{1-5}/C_3H_{0-3}N$ fragments at *m*/*z* 49−53, $C_3H_{0-3}/C_2H_{0-3}N$ fragments at *m*/*z* 36−41, NO (*m*/*z* 30), and $C_2H_{0-2}/CH_{0-2}N$ fragments *m*/*z* 24−28, in addition to loss of H (*m*/*z* 95) and OH (*m*/*z* 79). A further insight into the nature of these dissociations was obtained from the NR spectrum of $\mathbf{1a}^+$ (Figure 1b) that showed a very minor peak due to loss of H, peaks for losses of D (*m*/*z* 95) and OD (*m*/*z* 79), ring fragments at *m*/*z* 49−53, 36−41, and 24−29, and the peak of NO^+. Note that the ring fragments showed virtually no mass shifts due to the presence of deuterium. This

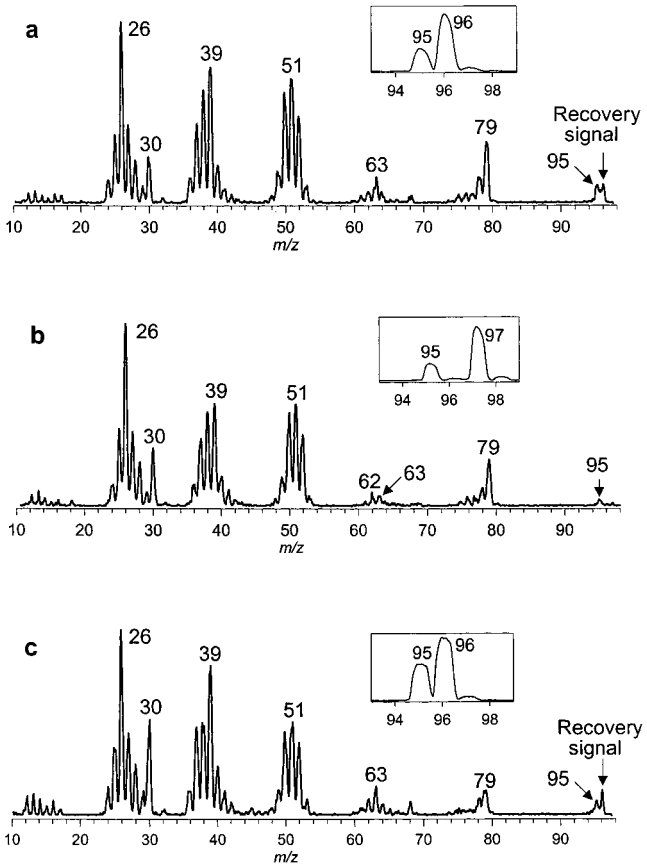

Figure 1. Neutralization (CH_3SSCH_3, 70% transmittance)/reionization (O_2, 70% transmittance) mass spectra of (a) $\mathbf{1}^+$and (b) $\mathbf{1a}^+$. (*c*) NR (CH_3SSCH_3/NO_2, 70% transmittance) mass spectrum of $\mathbf{1}^+$. Insets show the $(M + H)^+$ (*m*/*z* 96 in a and c) or $(M + D)^+$ (*m*/*z* 97 in b) regions in the corresponding chemical ionization mass spectra.

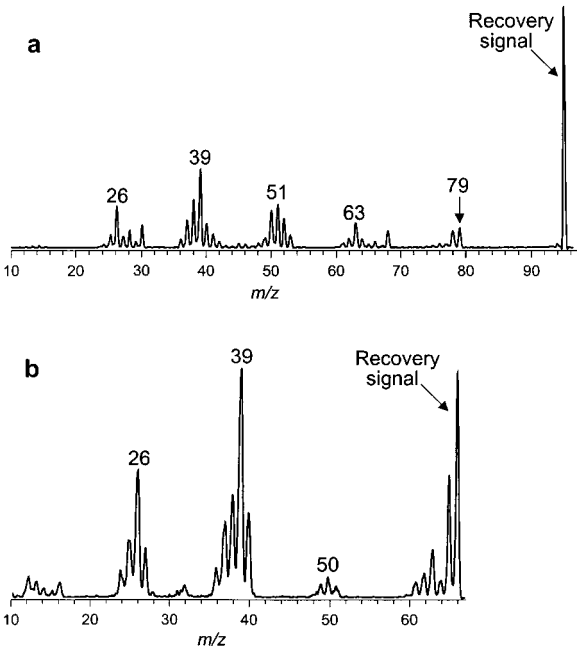

Figure 2. Neutralization (CH_3SSCH_3, 70% transmittance)/reionization (O_2, 70% transmittance) mass spectra of (a) $\mathbf{2}^{+\bullet}$ and (b) [cyclopentadiene]$^{+\bullet}$.

proved that the deuterium atom of the OD group was not mixed with the ring hydrogens and was directly lost as D or OD.

Consecutive dissociations of the presumed primary products, **2** and pyridine,[8b] respectively, were inferred from the reference NR spectra. The NR spectrum of $\mathbf{2}^{+\bullet}$ showed a prominent survivor ion at *m*/*z* 95 and ring fragments (Figure 2a). The relative abundance of the ring fragments in the NR spectrum of $\mathbf{2}^{+\bullet}$ (65% of the sum of NR peak intensities, ΣI_{NR}) was substantially less than that in the NR spectrum of **1** (>90% ΣI_{NR}). The NR spectrum of $[\text{pyridine}]^{+\bullet}$ also showed 65% ΣI_{NR} of ring-cleavage dissociations that formed fragments at *m*/*z* 49−52, 36−40, and 24−27.[8b] Hence, consecutive dissociations of pyridine, **2**, and their cation-radicals could qualitatively account for the ring-cleavage products observed in NR of $\mathbf{1}^+$. However, when scaled from the reference NR spectra, the contributions of pyridine and **2** dissociations amounted to only about 7 and 9%, respectively, of ring-cleavage products in NR of $\mathbf{1}^+$. Further excitation of neutral **2** by collisions with He caused more extensive ring fragmentations (spectrum not shown). For example, upon 50% attenuation due to collisions, the relative abundance of survivor $\mathbf{2}^{+\bullet}$ decreased from 29% ΣI_{NR} to 16% ΣI_{NR}, i.e., by 45%. This indicated that 100(45/50) ≈ 80% of collisions with He caused dissociation of neutral **2**, or in $\mathbf{2}^{+\bullet}$ following reionization. The energetics of these dissociations is discussed later in the paper.

The presence of an abundant peak of NO^+ by NR of **1** also indicated a dissociation pathway involving a ring cleavage. However, the complementary C_5H_6 fragment was very weak in the NR spectrum of **1**. A reference NR spectrum of cyclopentadiene was obtained that showed an abundant $C_5H_6^{+\bullet}$ survivor ion and $C_3H_3^+$ and $C_2H_2^{+\bullet}$ ring fragments (Figure 2b). Hence, the virtual absence of a $C_5H_6^{+\bullet}$ ion in NR of **1** suggested that NO was not produced by direct dissociation of **1** to cyclopentadiene + NO.

Collisional activation with oxygen can cause electronic excitation in the ion, thus supplying internal energy for highly endothermic dissociations, as reported recently.[30] A similar effect in collisional reionization of **1** with O_2 may provide excitation that could drive ring dissociations in $\mathbf{1}^+$. To check this possibility, we measured a NR spectrum of $\mathbf{1}^+$ using NO_2 for reionization instead of O_2 (Figure 1c). In contrast to O_2, NO_2 has no bound excited electronic states[31] and cannot promote resonant electronic excitation in the ion or neutral collision counterpart. The NR spectrum in Figure 1c was similar to that obtained by reionization with O_2 in that analogous abundant ring-cleavage dissociations were observed in both spectra. In addition, the CH_3SSCH_3/NO_2 NR mass spectrum showed an enhanced formation of NO^+ at *m*/*z* 30, while the pyridine ion at *m*/*z* 79 due to loss of OH was diminished. These effects on ion relative intensities can be due to some extent to different cross sections for collisional ionization with O_2 and NO_2 of the neutral fragments formed by dissociation of radical **1**.[32] However, the comparison of the CH_3SSCH_3/NO_2 and CH_3SSCH_3/O_2 NR mass spectra showed convincingly that the ring dissociations were determined mainly by the energetics of the electron-transfer producing the intermediate radical **1** and less so by collisional reionization.

To summarize the reaction types observed upon NR, ring cleavages were the predominant dissociations that competed with specific losses of OH and H from the N−OH group.

Ion Dissociations. Since neutral and post-reionization ion dissociations may overlap in NR mass spectra, ion dissociations pertinent to $\mathbf{1}^+$ were examined separately by collisionally activated dissociation (CAD) spectra (Table 2). CAD of $\mathbf{1}^+$ produced fragment ions due to losses of H (*m*/*z* 95), OH (*m*/*z* 79), H_2O (*m*/*z* 78), H + HCN (*m*/*z* 68), ring fragments at *m*/*z* 63, 50−52, and 37−41, and a weak peak of NO^+ at *m*/*z* 30.[33] The CAD spectrum of $\mathbf{1}^+$ differed substantially from the NR mass spectrum in the fragment relative intensities. In addition, deuterium labeling in $\mathbf{1a}^+$ revealed nearly statistical loss of H and D from the ion, as opposed to NR dissociations (vide supra). Thermochemical data[29] suggest that the main ion dissociations of $\mathbf{1}^+$ that were observed on CAD were substantially endothermic. For example, the formation of $[\text{pyridine}]^{+\bullet}$ + $OH^\bullet$ required 377 kJ mol^{-1} at the thermochemical threshold, and the formation of $\mathbf{2}^{+\bullet}$ + H required 420 kJ mol^{-1}.[34] Hence, the ion dissociation energetics differed dramatically from that of the radical, as discussed next.

TABLE 2: Collisionally Activated Dissociation Spectra of Ions $\mathbf{1}^+$, $\mathbf{1a}^+$, and $\mathbf{2}^{+\bullet}$. Relative Intensity[a]

m/*z*	$\mathbf{1}^+$	$\mathbf{1a}^+$	$\mathbf{2}^{+\bullet}$
26	1.9	2.3	0.7
27	1.0	1.9	0.2
28	1.4	1.7	0.4
29			0.2
30	1.2		0.7
36	0.9		0.2
37	2.3	2.4	1.2
38	4.3	2.7	3.4
39	9.0	4.1	7.9
40	2.4	2.1	3.6
41	1.6		2.6
42	1.1		0.7
48	3.0	1.7	0.5
48.5		6.6	
49	1.7	2.2	0.9
50	6.8	6.4	4.3
51	10.0	12.6	5.2
52	7.5	9.3	2.8
53	1.4	2.1	2.1
61	1.3		0.9
62	2.3		3.3
63	4.1	2.1	9.3
64	1.5	1.6	2.2
65	1.0		0.9
66	0.8		3.0
67	0.9		0.9
68	2.2		27.0
69	0.9		
75	0.8		0.2
76	0.8	1.8	0.5
77	0.7		
78	5.2	7.8	5.5
79	11.5	15.4	3.8
80	0.7		
94			4.5
95	6.3	2.8	
96		9.3	

[a] Relative to the sum of CAD ion intensities.

Radical Dissociation Energetics. To further elucidate the competing unimolecular dissociations of **1**, we obtained relative energies for several species and transition state energies for isomerizations and dissociations. The relevant energies from effective QCISD(T)/6-311+G(3df,2p) calculations are visualized in a potential energy diagram (Figure 3), and the relative energies obtained by B3-PMP2 calculations are summarized in Table 3. According to calculations, **1** was a local energy minimum of C_s symmetry in which the O−H bond was rotated out of the pyridine ring plane (Figure 4). However, **1** was metastable with respect to isomerization to the *ortho* and *para* nitroxyl radicals (**3** and **5**, respectively, Figure 3 and Table 3), *ortho*-, *meta*-, and *para*-hydroxydihydropyridyl radicals (**6**, **7**, and **8**, respectively), and dissociation by loss of OH to form

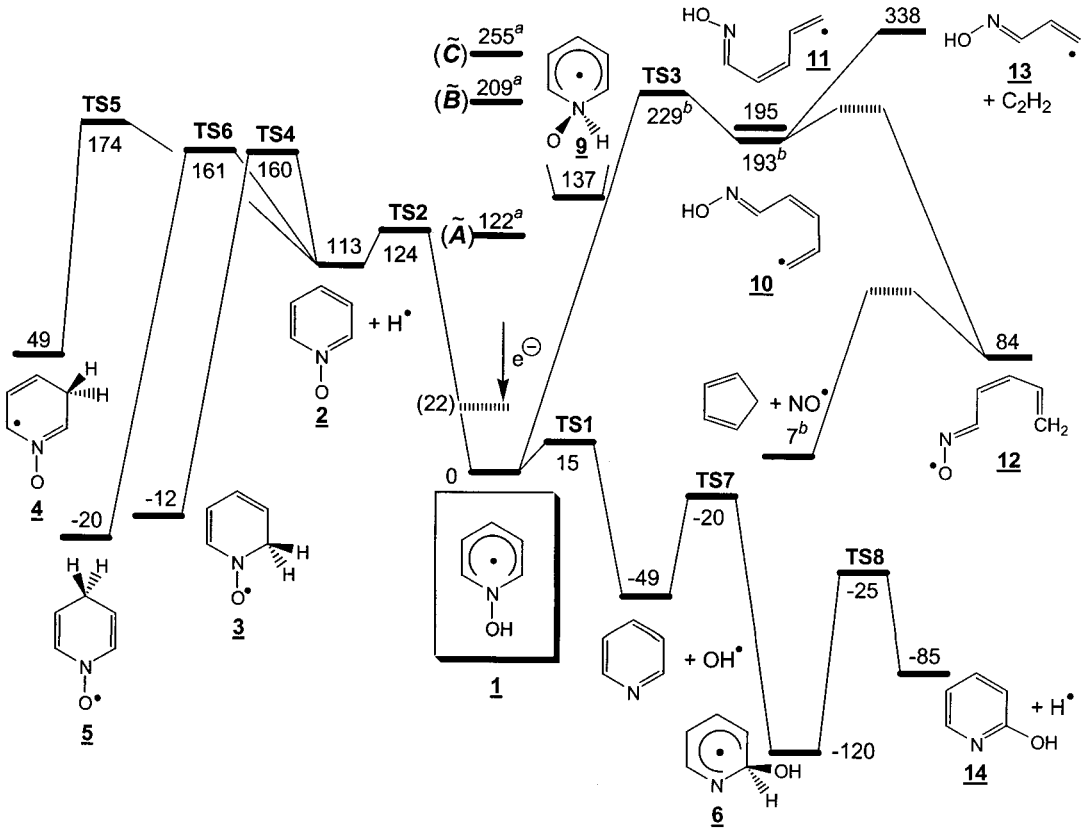

Figure 3. Potential energy diagram for dissociations and isomerizations of **1**. The relative energies are based on effective QCISD(T)/6-311+G-(3df,2p) total energies and B3LYP/6-31+G(d,p) zero-point corrections and refer to 0 K. [a]Excited state energies are from time-dependent B3LYP/6-311+G(2d,p) calculations. [b]These energies are based on the basis set expansions through the ROMP2 calculations.

TABLE 3: Relative Energies of (Pyridine + OH) Radicals

	energy[a]	
species	B3-MP2 6-311+G(3df,2p)	QCISD(T)[b] 6-311+G(3df,2p)
1	0	0
3	−20	−12
	1	−12
4	35	49
	48	44
5	−18	−20
	−1	−15
6	−114	−120
	−108	−120
7	−103	−108
	−97	−109
8	−95	−98
	−86	−99
9	144	139
	153	137

[a] In units of kJ mol^{-1} at 0 K. [b] PMP2 data in upper lines, ROMP2 data in lower lines. [c] Effective energies from basis set expansions.

pyridine. Radical **1** was more stable than the *meta*-nitroxyl radical **4** and the cyclic *N*-oxide radical **9** corresponding to hydrogen atom addition to N-1 in **2** (Table 3). The optimized structures of the isomeric radicals **3**−**9** and dissociation products **10**−**13** are shown in Figure 5, and the transition state geometries are shown in Figure 6.

Loss of the hydroxyl group from **1** was 49 kJ mol^{-1} exothermic and represented the lowest-energy dissociation path. Radical **1** gained modest kinetic stability from the 15 kJ mol^{-1} barrier to reach the transition state for cleavage of the N−O bond (**TS1**, Figure 3). The optimized structure of **TS1** (Figure 6) showed an early transition state in which the N−O bond was elongated by only 0.18 Å compared to the local minimum of **1** (Figure 4). For a radical produced by vertical electron capture, Franck−Condon effects alone induced 22 kJ mol^{-1} vibrational excitation which, in combination with the mean thermal energy of the precursor ion (38 kJ mol^{-1} at 523 K), should be more than sufficient to drive fast dissociation of **1**. In contrast, loss of the H atom from the OH group in **1** to produce **2** was 113 kJ mol^{-1} endothermic and included an additional small energy barrier (**TS2**). The dissociation and activation energies calculated at the other levels of theory are summarized in Table 4.

Reaction pathways for ring opening were studied in some detail to elucidate the ring dissociations observed on NR. Cleavage of the N−C-2 bond in **1** to give the open-ring intermediate **10** was 193 kJ mol^{-1} endothermic, and included an additional potential energy barrier in the transition state **TS3,** which was 36 kJ mol^{-1} above **10** (Figure 3). The **TS3** geometry showed a nearly in-plane cleavage of the N−C-2 bond (Figure 6), which must be followed by subsequent rotation about the C-5−C-6 bond to reach the *anti*−*anti*−*syn*−*syn* configuration of radical **10** (Figure 5).

Ring cleavages by C−C bond dissociations were also expected to lead to high-energy intermediates. A further dissociation of **10** by elimination of acetylene to form HC═CH−CH═N−OH (**13**) required 145 kJ mol^{-1} and may have involved an additional potential energy barrier. Note that the open-ring radical **10** can rearrange by hydrogen transfer to form the substantially more stable nitroxyl radical **12**, which, however, was still 84 kJ mol^{-1} above **1**. Radical **12** was a potential intermediate for the loss of NO from **1**.

Another possible pathway to losing NO was by isomerization to the more stable isomer **3** which can eliminate NO to form cyclopentadiene (Figure 3). The overall dissociation **1** → C_5H_6

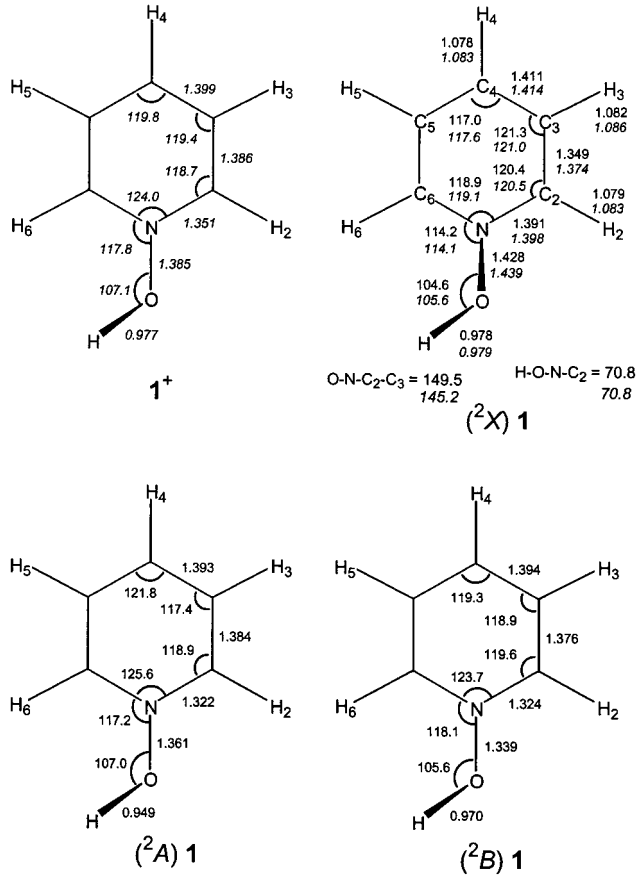

Figure 4. Optimized geometries of $\mathbf{1}^+$ and the X, A, and B electronic states of **1**. Roman numerals: UMP2/6-31+G(d,p) (^{2}X state) and UCIS/6-31+G(d,p) (^{2}A and ^{2}B states) geometries. Italics: B3LYP/6-31+G(d,p) geometries. Bond lengths in angstroms, bond and dihedral angles in degrees.

+ NO was only 7 kJ mol^{-1} endothermic and could, at least in principle, provide a low-energy pathway to ring-cleavage products. However, a search for the transition state for the **1** → **3** isomerization, which included migration of H from the OH group onto C-2, was unsuccessful. Upon decreasing the C-2•••H−O distance, the potential energy of the system increased steeply, and while the O−H bond showed a negligible elongation, the weak N−O bond was gradually stretched. At C-2••• H−O distances that would normally develop a bonding C−H interaction in the transition state (1.4−1.5 Å), the N−O bond dissociated completely, and the interaction between C-2 and the hydrogen end of the OH radical showed a negative (repulsive) energy gradient. This result indicated that, at the present level of theory at least, there was no low-lying cyclic transition state for the 1,3-hydrogen migration from **1** to **3**. A two-step isomerization by O−H bond dissociation followed by H atom addition to C-2 in **2** faced a large activation energy (160 kJ mol^{-1} above **1**, Figure 3) and should not occur in competition with loss of OH.

The calculations indicated that the low stability of **1**, as observed in the NR spectrum, can be explained by a facile OH loss which is promoted by vibrational excitation in **1** caused by a combination of the precursor ion thermal energy and Franck−Condon effects in vertical electron transfer. However, the calculated potential energy surface of the ground electronic state did not explain the loss of H and the extensive ring-cleavage dissociations observed upon NR.

Similar discrepancies between the predicted and observed dissociations have been noted previously for other heterocyclic radicals and attributed to the formation of excited electronic states upon collisional electron transfer.[8d,8e] An exited state can arise by electron capture in a vacant molecular orbital of the fast precursor ion, or by electron capture combined with excitation of a valence electron during collisional electron transfer. To be kinetically significant, the excited state must have a radiation lifetime commensurable with the dissociation lifetime, $t = 1/k$, where k is the unimolecular dissociation constant. To gain some insight, we investigated by computations the first five excited doublet states of **1**.

Electronic States of 1. The excitation energies and radiative lifetimes of the lowest five excited states in **1** were calculated at two levels of theory (UCIS and TD-B3LYP) for the optimized geometry of the ground electronic state, optimized geometries of the ^{2}A and ^{2}B states (Figure 4), and for **1** formed by vertical neutralization of $\mathbf{1}^+$ (Table 5). According to TD-B3LYP, the vertically formed ^{2}A state of **1** was 122 kJ mol^{-1} above the local minimum for the X state. The ^{2}A state was metastable with respect to loss of OH, and close to the energy of **TS2** for the loss of H from the OH group (Figure 3). The ^{2}B state was about 85 kJ mol^{-1} above **TS2**, but still 20 kJ mol^{-1} below **TS3** for ring opening in (^{2}X)**1**. Hence, internal conversion ^{2}B → ^{2}X could provide sufficient vibrational energy for **1** to dissociate by loss of H, but not for fast ring opening. The ^{2}C and higher excited states were above **TS3**, so that internal conversion ^{2}C → ^{2}X could provide energy for the vibrationally excited ^{2}X state to undergo ring cleavage. Note that the ^{2}C and ^{2}D states of **1** had radiative lifetimes of several microseconds (Table 5), and therefore could participate in state-selective dissociations or provide vibrational energy to the ^{2}X state following internal conversion.

In contrast, excited electronic states of the stable products pyridine and **2** were energetically inaccessible from the ^{2}A through ^{2}E excited states of **1**. For example, the vertical excitation energies of pyridine were calculated by TD-B3LYP as 3.9, 4.1, 4.5, and 4.8 eV for the ^{3}A$_1$, ^{3}B$_1$, ^{3}B$_2$, and ^{1}B$_1$ states, respectively, so that even a dissociation originating form a highly excited state, (^{2}E)**1** → (^{3}A$_1$) pyridine + OH•, was 12 kJ mol^{-1} endothermic. Likewise, the vertical excitation energies in **2** were calculated as 2.3, 3.5, 3.7, and 4.0 eV for the ^{3}A$_1$, ^{3}B$_2$, ^{3}A$_2$, and ^{1}A$_2$ states, respectively, which made the dissociation, (^{2}E)**1** → (^{3}A$_1$)**2** + H•, 38 kJ mol^{-1} endothermic. This indicated that excited electronic states of the primary products could be formed only from the sixth and higher excited states of **1**.

Ring-Cleavage Mechanisms in 1. What are the plausible mechanisms for ring-cleavage dissociations in NR of **1**? Some insights can be obtained from the dissociation energetics and results of labeling experiments. The energy diagram in Figure 3 suggests two different mechanisms which are now discussed. In the first mechanism, internal conversion in an excited state of **1** promotes dissociation by loss of H and OH. If the pyridine molecule is formed in a high vibrational state, its further dissociation can lead to ring-cleavage products, as shown previously by NRMS,[35] laser pyrolysis,[36] and shock-tube experiments.[37] The lowest-energy dissociation of neutral pyridine to 3-buten-1-yne and HCN requires 290 kJ mol^{-1} at the thermochemical threshold,[38] which can be supplied by dissociations originating from the ^{2}C and higher excited states of **1** (Figure 3). The lowest-energy dissociation of [pyridine]$^{+\bullet}$ to produce [methylenecyclopropene]$^{+\bullet}$ and HCN requires 310 kJ mol^{-1} threshold energy, which could be supplied by a combination of vibrational excitation in neutral pyridine produced from **1** and collisional excitation upon reionization. This leads to the

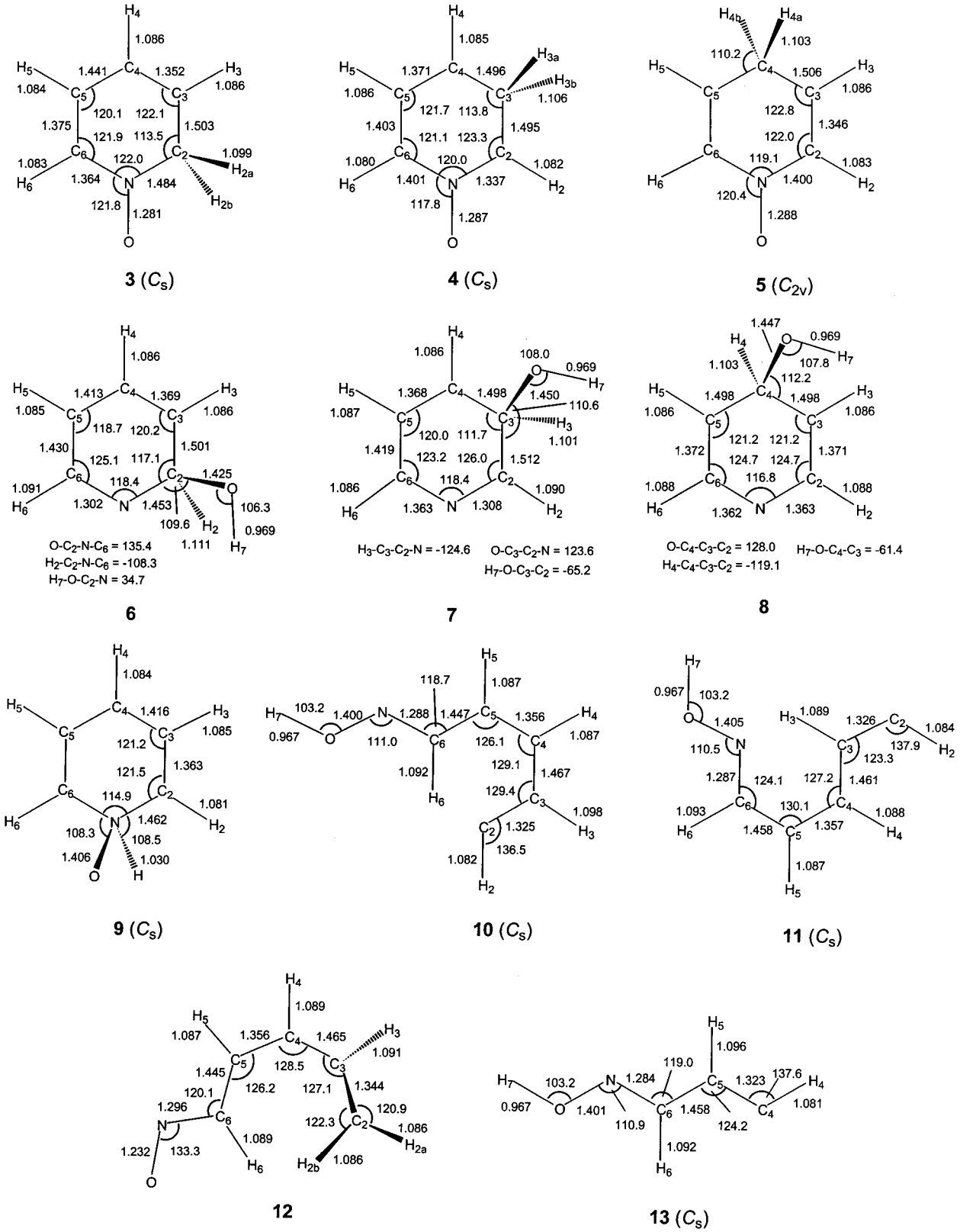

Figure 5. B3LYP/6-31+G(d,p) optimized geometries of **3**−**13**.

conclusion that post-reionization dissociations of [pyridine]$^{+\bullet}$ can result in extensive ring cleavages provided the *neutral molecule* was produced form **1** in highly excited vibrational states.

The energetics of **2** and **2**$^{+\bullet}$ also offer plausible mechanisms for ring cleavage dissociations. The reaction **2** → [cyclopentadienyl]$^{\bullet}$ + NO$^{\bullet}$ was calculated to be 214 kJ mol^{-1} endothermic, so that the formation of these products from **1** required 327 kJ mol^{-1}, which was only slightly above the energy of the vertically formed ^{2}E state of **1**. Dissociation by loss of NO from **2**$^{+\bullet}$ to produce the cyclopentadienyl cation was calculated to require 243 kJ mol^{-1} at 0 K, which could be readily supplied by a combination of vibrational excitation in **2** and further excitation upon collisional ionization. In keeping with the energy analysis,

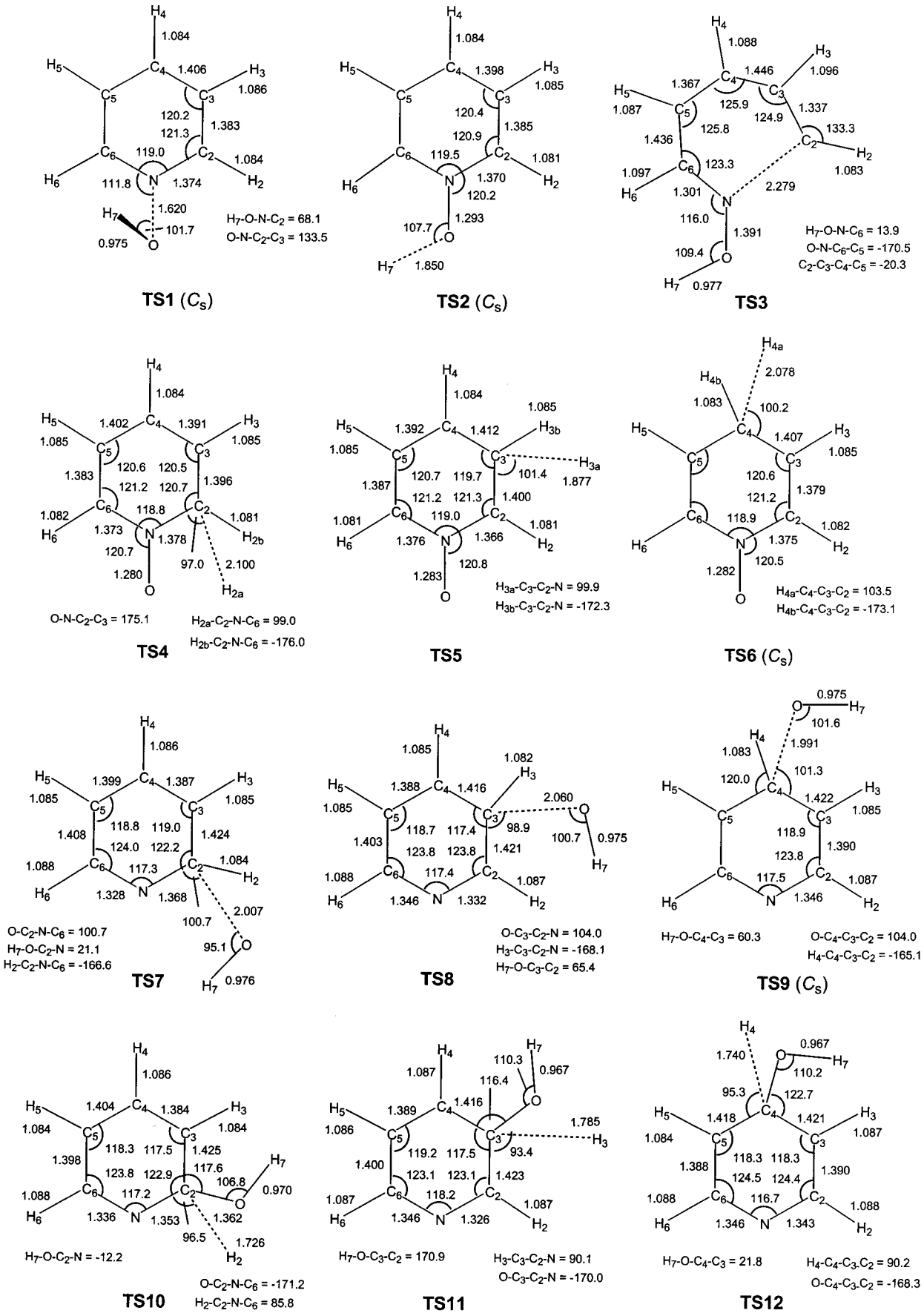

Figure 6. B3LYP/6-31+G(d,p) optimized geometries of transition states **TS1**−**TS12**.

collisional excitation of neutral **2** resulted in 80% ring-cleavage dissociations in excited **2** and/or $\mathbf{2}^{+\bullet}$.

To summarize the dissociation mechanisms, the generation upon vertical electron transfer of *excited electronic states* of **1**

TABLE 4: Dissociation and Activation Energies of (Pyridine + OH) Radicals

species/reaction	energy[a] B3-MP2[b] 6-311+G(3df,2p)	energy[a] QCISD(T)[b,c] 6-311+G(3df,2p)	species/reaction	energy[a] B3-MP2[b] 6-311+G(3df,2p)	energy[a] QCISD(T)[b,c] 6-311+G(3df,2p)
1 → **2** + H•	110	113	**5** → **TS6**	145	180
	118	120		134	173
1 → pyridine + OH•	−42	−49	**6** → **TS7**	82	100
	−32	−41	**7** → **TS8**	68	82
1 → **10**	193	225		71	84
	197	194	**8** → **TS9**	63	78
1 → **11**	199			70	81
	202		**6** → **14** + H•	29	35
1 → **12**	64	84		31	43
	85	84	**7** → **15** + H•	57	62
1 → **13** + C_2H_2	342	338		58	70
	349	338	**8** → **16** + H•	40	43
1 → cyclopentadiene + NO	12	−0.5		39	51
	21	7	**6** → **TS10**	78	95
1 → **TS1**	8	15		75	96
	1	12	**7** → **TS11**	103	120
1 → **TS2**	117	124		98	120
	125	132	**8** → **TS12**	89	91
1 → **TS3**	225	241		83	53
	235	236	pyridine + OH• → **TS1**	49	64
2 + H• → **TS2**	7	12		33	54
	8	13	pyridine + OH• → **TS7**	10	29
2 + H• → **TS4**	17	47	pyridine + OH• → **TS8**	6	23
	13	35		6	17
2 + H• → **TS5**	25	61	pyridine + OH• → **TS9**	11	29
	28	49		17	23
2 + H• → **TS6**	17	48	**14** + H• → **TS10**	49	60
	15	37		44	53
3 → **TS4**	147	172	**15** + H• → **TS11**	47	58
	129	167		41	50
4 → **TS5**	100	125	**16** + H• → **TS12**	48	48
	97	125		44	3

[a] In units of kJ mol^{-1} at 0 K. [b] PMP2 data in upper lines, ROMP2 data in lower lines. [c] Effective energies from basis set expansions.

TABLE 5: Excited State Energies of 1

species/geometry	state	excitation energy[a] UCIS[e]	excitation energy[a] TD-B3LYP[e]	f[b] UCIS[e]	f[b] TD-B3LYP[e]	t(μs)[c] UCIS[e]	t(μs)[c] TD-B3LYP[e]	configuration[d] UCIS	configuration[d] TD-B3LYP
(X) **1**	A	4.1	2.1	0.005	0.004	0.3	2.0	26α → 33α	26α → 27α
	B	4.8	3.1	0.027	0.034	0.04	0.07	26α → 27α	26α → 28α
	C	5.5	3.4	0.013	0.037	0.02	0.05	mixed α,β	26α → 29α
	D	5.5	3.8	0	0	>20	>20	26α → 28α	26α → 30α
	E	5.7	4.0	0.043	0.012	0.02	0.1	mixed α,β	26α → 31α
1 (VN)[f]	A	2.9 (3.3)[g]	1.0 (1.3)[g]	0.002	0.002	1.1	12	26α → 33α	26α → 27α
	B	3.5 (3.9)	1.9 (2.1)	0.03	0.02	0.06	0.3	26α → 27α	26α → 28α
	C	4.1 (4.5)	2.4 (2.6)	0.002	0.002	0.5	2.5	mixed α	26α → 29α
	D	4.3 (4.7)	2.9 (3.1)	0.001	0.001	2.1	4	26α → 28α	26α → 30α
	E	4.6 (5.0)	3.2 (3.4)	0.003	0.005	0.4	0.4	mixed α	26α → 31α
(A) **1**	A	2.6 (3.2)[g]	0.8 (1.3)[g]	0.002	0.001	1.9	24	26α → 33α	26α → 27α
	B	3.2 (3.8)	1.8 (2.3)	0.04	0.03	0.06	0.2	26α → 27α	26α → 28α
	C	4.0 (4.6)	2.3 (2.8)	0.007	0.003	0.2	1.6	mixed α	26α → 29α
	D	4.4 (5.0)	2.7 (3.2)	0.001	0.001	2.0	3.9	26α → 28α	26α → 30α
	E	4.5 (5.1)	3.1 (3.5)	0.002	0.005	0.6	0.6	mixed α	26α → 31α
(B) **1**	A	2.6 (3.2)[g]	1.0 (1.4)[g]	0.002	0.002	1.6	16	26α → 33α	26α → 27α
	B	3.2 (3.8)	1.8 (2.2)	0.037	0.03	0.06	0.2	26α → 27α	26α → 28α
	C	4.0 (4.6)	2.4 (2.9)	0.007	0.003	0.2	1.5	mixed α	26α → 29α
	D	4.1 (4.7)	2.8 (3.2)	0.001	0.001	1.7	2.8	26α → 28α	26α → 30α
	E	4.4 (5.0)	3.1 (3.6)	0.003	0.005	0.5	0.5	mixed α	26α → 31α

[a] In units of electronvolts relative to the ground state of the pertinent optimized geometry. [b] Oscillator strength. [c] Radiative lifetime for transition to the ground state. [d] Dominant configurations with expansion coefficients >0.8. [e] Calculations with the 6-311+G(2d,p) basis set. [f] Vertical neutralization of cation **1**$^+$. [g] Excitation energies relative to the optimized ground state of **1**.

TABLE 6: Kinetic Parameters for OH Additions to Pyridine

method		position			
		N	C-2,C-6[a]	C-3,C-5[a]	C-4
QCISD(T)/6-311+G(3df,2p)	E_{TS}[b]	64.0	28.9	23.1	29.3
	E_a[c]	67.2	32.8	27.6	33.5
	log A[d]	11.69	12.11	12.44	12.34
	log k_{200}[e]	−5.83	3.57	5.27	3.62
	log k_{298}	−0.11	5.35	7.59	6.45
	log $k_{rel,298}$[f]	0[g]	0.052	0.915	0.033
	log $k_{total,298}$[h]		7.65		
B3−PMP2/6-311+G(3df,2p)	E_{TS}	49.4	9.8	6.5	10.6
	E_a	52.6	13.8	10.9	14.8
	log A	11.69	12.11	12.44	12.34
	log k_{200}	-2.02	8.56	9.63	8.50
	log k_{298}	2.46	9.69	10.52	9.73
	$k_{rel,298}$	0[g]	0.122	0.812	0.066
	log $k_{total,298}$		10.64		
B3−PMP2/6-311+G(2d,p)	E_{TS}	54.3	10.2	6.7	10.8
	E_a	57.4	14.1	11.1	15.1
	log A	11.69	12.11	12.44	12.34
	log k_{200}	−3.28	8.46	9.58	8.44
	log k_{298}	1.61	9.63	10.48	9.69
	$k_{rel,298}$	0[g]	0.115	0.820	0.065
	log $k_{total,298}$		10.60		
B3−ROMP2/6-311+G(2d,p)	E_{TS}	38.6	16.3	7.6	17.7
	E_a	41.8	20.3	12.0	22.0
	log A	11.69	12.11	12.44	12.34
	log k_{200}	0.81	6.86	9.34	6.63
	log k_{298}	4.35	8.55	10.32	8.47
	$k_{rel,298}$	0[g]	0.016	0.977	0.007
	log $k_{total,298}$		10.34		
experiment	E_a		6.3 ± 0.8[i]		
	log A		12.32 ± 0.17		
	log k_{total}		11.21 ± 0.22[i,j]		
			10.98[k]		

[a] Total fractions for additions to the equivalent C-2/C-6 and C-3/C-5 positions. [b] Calculated activation energies for OH additions in kJ mol^{-1}. [c] Arrhenius activation energies in kJ mol^{-1}. [d] Arrhenius preexponential factors. [e] Bimolecular rate constants mol^{-1} cm^3 s^{-1} at the indicated absolute temperatures. [f] Relative rate constants, $k_{rel} = k/(k_N + k_{C-2} + k_{C-3} + k_{C-4})$. [g] Relative rate constants $<10^{-6}$. [h] From log($k_N + k_{C-2,C-6} + k_{C-3,C-5} + k_{C-4}$). [i] Corresponds to total OH additions. [j] At 298 K from ref 7a. [k] At 297 K from ref 7b.

provides the energy to drive dissociations forming vibrationally excited pyridine and **2**. The latter molecule, and its cation radical in particular, can dissociate by expulsion of NO and other ring-cleavages to produce the various fragments observed in the NR spectrum of **1**.

Hydroxyl Radical Addition to Pyridine. The calculated transition state energies allowed us to assess the kinetics of bimolecular hydroxyl radical additions to the N-1, C-2, C-3, and C-4 positions in pyridine, which were relevant to the previous pulse radiolysis[4] and gas-phase studies.[7] The calculated rate constants and activation parameters are summarized in Table 6. As expected, the absolute rate constants strongly depended on the transition state energies, which in turn depended on the computational scheme used. However, *relative rate constants* showed similar trends regardless of the level of theory used. The symmetrically equivalent positions C-3/C-5 in pyridine showed the lowest activation energies for OH addition and were therefore most reactive. OH additions to C-3/C-5 amounted to 81−98% of total reactivity, when expressed as the pertinent relative rate constant, k_{rel} (Table 6). The k_{rel} values for OH addition to the C-2/C-6 and C-4 positions were similar, so that an OH attack in the ortho-positions was predicted to be favored for statistical reasons. The nitrogen atom was calculated to be virtually unreactive toward OH attack.

These predicted relative rate constants were in very good qualitative agreement with previous experimental results.[4] Analysis of the reaction products following pulse radiolysis of pyridine indicated that >80% of OH attacks took place in the C-3 and C-5 positions, which is reproduced by the present calculations. In addition, no **2** was detected in the reaction mixture following pulse radiolysis,[4c] which is consistent with the high calculated energy barrier for an OH attack at the pyridine nitrogen atom.

The calculated total rate constants, $k_{total} = k_N + k_{C-2,C-6} + k_{C-3,C-5} + k_{C-4}$, varied greatly (Table 6). In general, the gas-phase rate constants calculated at the present levels of theory were lower than the experimental values. The best match was obtained for the rate constant calculated from the B3−PMP/6-311+G(3df,2p) transition state energy which also showed the best match with the experimental Arrhenius activation energy (6.3 kJ mol^{-1}, Table 6). Using the smaller 6-311+G(2d,p) basis set gave acceptable kinetic data when based on B3-PMP2 and B3-ROMP2 transition state energies. This is significant for transition state calculations of yet larger open-shell systems for which the 6-311+G(3df,2p) basis set could be prohibitively expensive. Note also that the log A terms were predicted accurately from the calculated partition functions (Table 6).

It may also be noted that the transition state energies obtained at the present levels of theory were greater than those reported recently from B3LYP calculations which predicted a negative activation energy for the OH addition to C-3 in pyridine.[39] That result was likely to be an artifact of B3LYP calculations that were reported to underestimate activation energies in radical additions to several unsaturated systems.[40]

Hydrogen Atom Addition to Pyridine-*N*-oxide. Hydrogen atoms are produced by pulse radiolysis of water,[2] and their reactivity toward pyridine derivatives is also of interest. The potential energy diagram in Figure 3 suggests that H atom

SCHEME 2

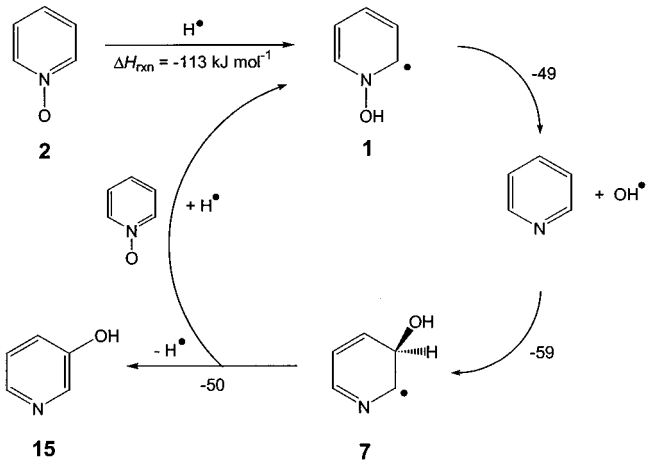

addition in **2** should proceed preferentially at the O atom to form **1**. H atom additions to the C-2 through C-4 positions in **2** showed substantially higher activation energies and should not compete effectively with the addition at oxygen. However, an H addition forming **1** was 110−113 kJ mol−1 exothermic, so that the radical adduct was expected to be vibrationally excited above the potential energy barrier for the exothermic OH loss. The overall exothermicity of the reaction **2** + H• → pyridine + OH•, $\Delta H_{rxn} = -162$ kJ mol^{-1}, indicated that **2** should be susceptible to facile reduction by H atoms. More interestingly, the readdition of the OH radical formed by the dissociation of intermediate **1** can occur exothermically in the C-2, C-3, and C-4 positions (vide supra), and the respective intermediate radicals **7**−**9** can subsequently transfer a hydrogen atom to another molecule of **2** to produce stable hydroxypyridines (**14**−**16**) while recreating **1**. This is shown for 3-hydroxypyridine (**15**) in Scheme 2, which also gives the calculated reaction enthalpies in kJ mol^{-1}. The analogous reactions with **2** of radicals **6** and **8** were 71 and 70 kJ mol^{-1} exothermic, respectively. These reaction sequences thus could create *catalytic cycles* for isomerizations of **2** to hydroxypyridines **14**−**16**, which are triggered by the hydrogen atom addition to **2** and driven by exothermic OH additions to pyridine and H atom transfers to **2**. The catalytic cycle shown in Scheme 2 can possibly provide an efficient mechanism for destruction of **2** and may explain the absence of **2** in the mixtures produced by pulse radiolysis of pyridine.[4c]

Conclusions

N-hydroxypyridyl radical **1** is a highly reactive species that has been transiently generated for the first time by femtosecond collisional electron transfer in the gas phase. The radical is only weakly bound with respect to dissociation to pyridine and OH radical. In addition to the predicted loss of OH, **1** produced by collisional electron transfer also underwent specific loss of H that originated from excited electronic states. While the energetics of OH additions to pyridine exclude **1** as an intermediate, it can play a pivotal role in catalytic isomerization of pyridine-*N*-oxide to the more stable hydroxypyridines.

Acknowledgment. This work was supported by a grant from the National Science Foundation (CHE-0090930). We thank Dr. Martin Sadilek for technical assistance with CAD spectra measurements and Mr. Erik Syrstad for helpful discussions.

References and Notes

(1) Atkinson, R. Kinetics and Mechanisms of the Gas-Phase Reactions of the Hydroxyl Radical with Organic Compounds. In *Journal of Physical Chemistry Reference Data, Monograph No. 1*; American Chemical Society: New York, 1989; p 192.

(2) von Sonntag, C. In *Physical and Chemical Mechanisms of Molecular Radiation Biology*; Glass, W. A., Varma, M. N., Eds.; Plenum Press: New York, 1991; pp 287−321.

(3) Richter, C. In *Free Radical Toxicology*; Wallace, K. B., Ed.; Taylor and Francis: Washington, DC, 1997.

(4) (a) Steenken, S.; O'Neill, P. *J. Phys. Chem.* **1978**, *82*, 372. (b) Cohem, H.; Meyerstein, D. *J. Chem. Soc., Dalton Trans.* **1976**, 1976. (c) Selvarajan, N.; Raghavan, N. V. *J. Phys. Chem.* **1980**, *84*, 2548.

(5) Katritzky, A. R.; Johnson, C. D. *Angew. Chem., Int. Ed. Engl.* **1967**, *6*, 608.

(6) Anthony, M. C.; Waltz, W. L.; Mezey, P. G. *Can. J. Chem.* **1982**, *60*, 813.

(7) (a) Atkinson, R.; Tuazon, E. C.; Wallington, T. J.; Aschmann, S. M.; Arey, J.; Winer, A. M.; Pitts, J. N., Jr. *Environ. Sci. Technol.* **1987**, *21*, 64. (b) Witte, F.; Zetzsch, C. Unpublished results cited in ref 7a.

(8) (a) Nguyen, V. Q.; Turecek, F. *J. Mass Spectrom.* **1996**, *31*, 1173. (b) Nguyen, V. Q.; Turecek, F. *J. Mass Spectrom.* **1997**, *32*, 55. (c) Nguyen, V. Q.; Turecek, F. *J. Am. Chem. Soc.* **1997**, *119*, 2280. (d) Wolken, J. K.; Turecek, F. *J. Phys. Chem. A* **1999**, *103*, 6268. (e) Wolken, J. K.; Turecek, F. *J. Am. Chem. Soc.* **1999**, *121*, 6010.

(9) For the most recent reviews, see: (a) Zagorevskii, D. V.; Holmes, J. L. *Mass Spectrom. Rev.* **1999**, *18*, 87. (b) Schalley, C. A.; Hornung, G.; Schroder, D.; Schwarz, H. *Chem. Soc. Rev.* **1998**, *27*, 91. (c) Turecek, F. *J. Mass Spectrom.* **1998**, *33*, 779.

(10) Turecek, F.; Gu, M.; Shaffer, S. A. *J. Am. Soc. Mass Spectrom.* **1992**, *3*, 493.

(11) Turecek, F. *Org. Mass Spectrom.* **1992**, *27*, 1087.

(12) Frisch, M. J.; Trucks, G. W.; Schlegel, H. B.; Scuseria, G. E.; Robb, M. A.; Cheeseman, J. R.; Zakrzewski, V. G.; Montgomery, J. A., Jr.; Stratmann, R. E.; Burant, J. C.; Dapprich, S.; Millam, J. M.; Daniels, A. D.; Kudin, K. N.; Strain, M. C.; Farkas, O.; Tomasi, J.; Barone, V.; Cossi, M.; Cammi, R.; Mennucci, B.; Pomelli, C.; Adamo, C.; Clifford, S.; Ochterski, J.; Petersson, G. A.; Ayala, P. Y.; Cui, Q.; Morokuma, K.; Malick, D. K.; Rabuck, A. D.; Raghavachari, K.; Foresman, J. B.; Cioslowski, J.; Ortiz, J. V.; Stefanov, B. B.; Liu, G.; Liashenko, A.; Piskorz, P.; Komaromi, I.; Gomperts, R.; Martin, R. L.; Fox, D. J.; Keith, T.; Al-Laham, M. A.; Peng, C. Y.; Nanayakkara, A.; Gonzalez, C.; Challacombe, M.; Gill, P. M. W.; Johnson, B.; Chen, W.; Wong, M. W.; Andres, J. L.; Gonzalez, C.; Head-Gordon, M.; Replogle, E. S.; Pople, J. A. *Gaussian 98*, revision A.6, Gaussian, Inc.: Pittsburgh, PA, 1998.

(13) (a) Becke, A. D. *J. Chem. Phys.* **1993**, *98*, 1372, 5648. (b) Stephens, P. J.; Devlin, F. J.; Chabalowski, C. F.; Frisch, M. J. *J. Phys. Chem.* **1994**, *98*, 11623.

(14) (a) Rauhut, G.; Pulay, P. *J. Phys. Chem.* **1995**, *99*, 3093. (b) Finley, J. W.; Stephens, P. J. *J. Mol. Struct. (THEOCHEM)* **1995**, *227*, 357. (c) Wong, M. W. *Chem. Phys. Lett.* **1996**, *256*, 391.

(15) Scott, A. P.; Radom, L. *J. Phys. Chem.* **1996**, *100*, 16502.

(16) Møller, C.; Plesset, M. S. *Phys. Rev.* **1934**, *46*, 618.

(17) (a) Schlegel, H. B. *J. Chem. Phys.* **1986**, *84*, 4530. (b) Mayer, I. *Adv. Quantum Chem.* **1980**, *12*, 189.

(18) McWeeny, R.; Diercksen, G. *J. Chem. Phys.* **1968**, *49*, 4852.

(19) Parkinson, C. J.; Mayer, P. M.; Radom, L. *J. Chem. Soc., Perkin Trans. 2* **1999**, 2305.

(20) Turecek, F. *J. Phys. Chem. A* **1998**, *102*, 4703.

(21) (a) Turecek, F.; Wolken, J. K. *J. Phys. Chem. A* **1999**, *103*, 1905. (b) Turecek, F.; Carpenter, F. H. *J. Chem. Soc., Perkin Trans. 2* **1999**, 2315. (c) Turecek, F.; Polasek, M.; Frank, A. J.; Sadilek, M. *J. Am. Chem. Soc.* **2000**, *122*, 2361. (d) Polasek, M.; Turecek, F. *J. Am. Chem. Soc.* **2000**, *122*, 9511. (e) Polasek, M.; Turecek, F.; Gerbaux, P.; Flammang, R. *J. Phys. Chem. A* **2001**, *105*, 995.

(22) Rablen, P. R. *J. Am. Chem. Soc.* **2000**, *122*, 357.

(23) Pople, J. A.; Head-Gordon, M.; Raghavachari, K. *J. Chem. Phys.* **1987**, *87*, 5968.

(24) Curtiss, L. A.; Raghavachari, K.; Pople, J. A. *J. Chem. Phys.* **1993**, *98*, 1293.

(25) (a) Curtiss, L. A.; Redfern, P. C.; Smith, B. J.; Radom, L. *J. Chem. Phys.* **1996**, *104*, 5148. (b) Smith, B. J.; Radom, L. *J. Phys. Chem.* **1995**, *99*, 6468.

(26) Foresman, J. B.; Head-Gordon, M.; Pople, J. A.; Frisch, M. J. *J. Phys. Chem.* **1992**, *96*, 135.

(27) Stratmann, R. E.; Scuseria, G. E.; Frisch, M. J. *J. Chem. Phys.* **1998**, *109*, 8218.

(28) The calculated thermochemical proton affinity of **2** (920 kJ mol^{-1}, Table 1) was in a good agreement with the tabulated experimental values (922−924 kJ mol^{-1}, ref 29).

(29) (a) Lias, S. G.; Liebman, J. F.; Levin, R. D. *J. Phys. Chem. Ref. Data* **1984**, *13*, 695. (b) *NIST Standard Reference Database No. 69*; National Institute of Standards and Technology: Gaithersburg, MD, February 2000 (http://webbook.nist.gov/chemistry).

(30) Aubry, C.; Holmes, J. L. *J. Am. Soc. Mass Spectrom.* **2001**, *12*, 23.

(31) Busch, G. E.; Wilson, K. R. *J. Chem. Phys.* **1972**, *56*, 3626.

(32) Small amounts of NO^+ in the CH_3SSCH_3/NO_2 NR spectrum of **1** could be produced by dissociative collisional ionization of NO_2 by the keV neutral beam in a narrow region of potential gradient (−2500 to −2550 V) outside the reionization collision chamber (ref 11).

(33) Flammang, R.; Henrotte, V.; Gerbaux, P.; Nguyen, M. T. *Eur. Mass Spectrom.* **2000**, *6*, 3.

(34) From the pertinent enthalpies of formation: $\Delta H_{f,298}$ (kJ mol^{-1}) of $\mathbf{1}^+$ (696), [pyridine$^{+\bullet}$] (1034), $\mathbf{2}^{+\bullet}$ (896), OH (39), and H (218), ref 29.

(35) Turecek, F.; Wolken, J. K.; Sadilek, M. *Eur. Mass Spectrom.* **1998**, *4*, 321.

(36) Hore, N. R.; Russell, D. K. *J. Chem. Soc., Perkin Trans. 2* **1998**, 269.

(37) Kiefer, J. H.; Zhang, Q.; Kern, R. D.; Yao, J.; Jursic, B. *J. Phys. Chem.* **1990**, *94*, 4099.

(38) From the enthalpies of formation, $\Delta H_{f,298} = 140$, 135, and 295 kJ mol^{-1} for pyridine, HCN, and but-1-yne-3-ene, respectively (ref 29b).

(39) Barckholtz, C.; Barckholtz, T. A.; Hadad, C. M. *J. Phys. Chem. A* **2001**, *105*, 140.

(40) See, for example: (a) Nguyen, M. T.; Creve, S.; Vanquickenborne, L. G. *J. Phys. Chem.* **1996**, *100*, 18422. (b) Rice, B. M.; Pai, S. V.; Chabalowski, C. F. *J. Phys. Chem. A* **1998**, *102*, 6950. (c) Rassolov, V. A.; Ratner, M. A.; Pople, J. A. *J. Chem. Phys.* **2000**, *112*, 4014. (d) Lynch, B. J.; Fast, P. L.; Harris, M.; Truhlar, D. G. *J. Phys. Chem. A* **2000**, *104*, 4811.